Conceptual Designs of 50MW$_e$ and 450MW$_e$ Supercritical CO$_2$ Turbomachinery Trains for Power Generation from Coal. Part 1: Cycle and Turbine

Rahul A. Bidkar [a], Andrew Mann [a], Rajkeshar Singh [a], Edip Sevincer [a], Stefan Cich [b], Meera Day [b], Chris D Kulhanek [b], Azam M Thatte [a], Andrew M. Peter [a], Doug Hofer [a], Jeff Moore [b]

(a) General Electric Company, GE Global Research, One Research Circle, Niskayuna, NY 12309 USA
(b) Southwest Research Institute, P.O. Box 28510, Division 18, San Antonio, TX 78228 USA

ABSTRACT

Supercritical CO$_2$ power cycles could be a more efficient alternative to steam Rankine cycles for power generation from coal. However, CO$_2$ turbomachinery for this application has not yet been designed. This paper summarizes a scale-up of the 10MW$_e$ Southwest Research Institute (SwRI) and General Electric (GE) Sunshot CO$_2$ turbine design to the maximum size possible, nominally about 50MW$_e$. The thermodynamic cycle and turbine design are described. This non-reheat recompression cycle can achieve >49% cycle efficiency at ISO conditions with wet cooling. Scale-up of the Sunshot turbine beyond 50MW$_e$ is limited by the availability of long, large diameter rotor forgings and requires a change to an assembled rotor design. A clean-sheet conceptual design of a 450MW$_e$ assembled turbine rotor is also presented. It appears possible to package this reheat turbine rotor into a single casing at 3600 rpm and still maintain rotordynamic stability. This reheat recompression cycle can achieve 51.9% cycle efficiency. To achieve this high efficiency, a key turbomachinery technology gap is large-diameter film-riding end seals. On the system side, efficient recovery of the flue gas thermal energy with >500°C CO$_2$ feed temperature is required to translate the high cycle efficiency into a high net plant efficiency.

1. INTRODUCTION

Closed-loop recompression Brayton cycles using supercritical carbon dioxide (sCO$_2$) as a working fluid have been proposed to replace steam for power generation from pulverized coal [1]. The primary benefit to using sCO$_2$ as a working fluid in such a cycle is that it can achieve higher thermal cycle efficiency (up to 5 points [1]) at the equivalent turbine inlet conditions of state-of-the-art ultrasupercritical steam plants. This efficiency gain is due to the transfer of thermal energy from coal combustion to the sCO$_2$ power cycle at a higher average temperature than in a comparable steam cycle. Additional benefits include reduced water consumption, reduced power block size (smaller turbomachinery and condenser due to the higher working fluid density), and better thermodynamic integration with post-combustion CO$_2$ capture and compression equipment as shown by Moullec [1]. These benefits make sCO$_2$ turbomachinery an attractive possibility for power generation. In this Part-1 paper, optimized thermodynamic cycles for indirectly-fired sCO$_2$ power plants are presented for 50 MW$_e$ and 450 MW$_e$ scales along with turbine layouts for these scales. In a companion Part-2 paper [2],

compressor and recompressor layouts intended for direct coupling with the 450 MW$_e$ turbine are presented. The turbine layout discussed in this Part-1 paper and the compressor/recompressor layout discussed in the Part-2 paper [2] together are intended to demonstrate feasibility of an indirectly-fired utility-scale coal-based power plant with sCO$_2$ as the working fluid.

Turbomachinery development for large-scale SCO$_2$ recompression cycles is still in its infancy. The state-of-the-art development has been focused on integrated system-level demonstration at small scales (<1MW), and on turbomachinery development at intermediate scale (nominally 10MW). The RCBC at Sandia National Laboratories [3] and the IST at Bechtel Marine Propulsion Corporation [4] are examples of small-MW scale (< 1 MW) integrated recompression Brayton cycle demonstration loops. Apart from these small-MW scale efforts, there are two intermediate-scale sCO$_2$ turbomachinery development programs: the Echogen EPS100 for waste heat recovery applications [5] and the General Electric (GE) Sunshot expander for concentrated solar power (CSP) applications developed under the Southwest Research Institute (SwRI) and GE Sunshot program [6, 7]. The EPS100 utilizes radial inflow turbines to generate nominally 8 MW$_e$ gross from a 530°C gas turbine exhaust waste heat source [5]. Radial turbine technology is not likely to be optimal for multi-100MW utility-scale coal-fired power generation plants [8]. The SwRI/GE Sunshot program [6, 7] is therefore developing axial expander technology with 715°C turbine inlet temperatures for CSP power generation. In this paper, the SwRI/GE Sunshot turbine architecture [6, 7] is extended to 50 MW$_e$ scale to demonstrate scalability of the design to such intermediate power scales. Furthermore, limitations of this intermediate-scale turbine architecture are discussed in the context of utility scales (nominally 500 MW$_e$) and a clean sheet turbine layout is presented for the 450 MW$_e$ scale.

The turbine layouts for the 50 MW$_e$ and the 450 MW$_e$ scale presented in this paper are a result of several design considerations. These include thermodynamic cycle optimization, material considerations, turbine flow-path optimization, mechanical stress calculations and rotordynamic stability considerations. In this paper, these design considerations are discussed along with their interactions. The design process is constrained by availability of materials (both size limitations and strength limitations), lack of maturation in key technologies like turbine end seals or high-temperature furnace regenerative air preheaters. Such limitations in current technology and their role in enabling sCO$_2$ cycles for utility-scale power generation are also discussed in this paper.

The design process starts with a thermodynamic cycle with assumed performances for the power plant components including turbines, compressors and heat exchangers (heaters, recuperators, condensers). The thermodynamic cycles for both the 50 MW$_e$ and the 450 MW$_e$ designs are discussed in Section 2. The thermodynamic cycle optimization allows the computation of overall thermodynamic cycle efficiency. Additionally, it provides flow conditions and efficiency specifications that act as a starting point for design of individual components including turbines and compressors. In Section 3, aerodynamic flow-path optimization is presented for the 50 MW$_e$ and 450 MW$_e$ designs. Rotor material availability, manufacturability and gearbox availability play a key role in determining the aerodynamic flow-path architecture. These constraints are discussed in Section 3 along with the architecture differences between the 50 MW$_e$ and the 450 MW$_e$ turbines. In Section 4, mechanical design calculations, axial sizing calculations and rotordynamic studies are presented for the turbine rotors. Key technologies needed for enabling sCO$_2$ cycles for utility-scale power generation are highlighted in Section 5. Finally, a summary of the present work is described in Section 6.

2. THERMODYNAMIC CYCLE DESIGN

In this section, the assumptions and the underlying recompression cycle used for the turbine layout design are described. The thermodynamic cycle performance is sensitive to the main compressor inlet conditions, which can change depending on the ambient conditions and cooling system. The site assumptions are taken from the U.S. Dept. of Energy fossil-energy performance baseline document [9], which defines a greenfield Midwestern USA site with ISO design point conditions (15°C, 60% relative humidity) and mechanical draft evaporative cooling towers as a baseline plant. At these conditions, CO_2 can be condensed prior to the main compressor inlet. Another crucial assumption is that there are no integration constraints imposed on the power cycle design by the furnace, emissions cleanup, or any future potential carbon capture systems. Specifically, it is assumed that furnace design with high CO_2 feed temperatures is possible. Furthermore, the power cycle is designed to maximize thermodynamic cycle efficiency (the efficiency of perfect adiabatic heat addition converted to electric power) without any restrictions on the primary heater caused by the present unavailability of high-temperature air preheaters. High-temperature regenerative air preheaters are a key technology gap that would affect the overall plant cycle efficiency, but this specific technology gap is not addressed in the present work.
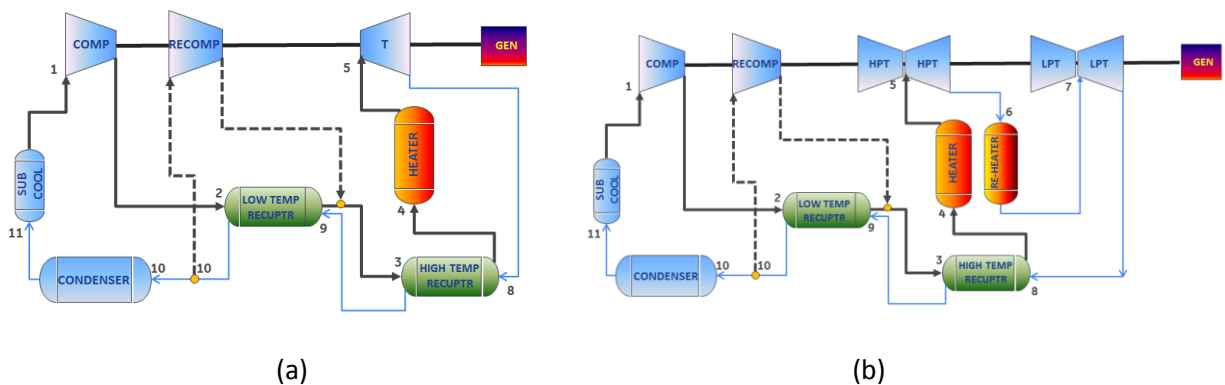

(a)   (b)

Figure 1 (a) Recompression cycle for the 50 MW$_e$ turbine, and (b) recompression cycle with reheat for the 450 MW$_e$ turbine. Note that the relative position of turbines and compressors as shown above is different from the actual single-shaft layout. COMP - main compressor, RECOMP - recompressor, T - turbine, GEN -generator, RECUPTR - recuperator, HPT – high-pressure turbine, LPT – low-pressure turbine

The thermodynamic cycle modeling was performed using Aspen HYSYS V8.6 with REFPROP as the fluid package. In Figure 1a, a simplified recompression CO_2 cycle is shown for the 50MW$_e$ turbine, while in Figure 1b, a reheat recompression CO_2 cycle is shown for the 450 MW$_e$ turbine. Starting at the main compressor inlet (state 1) CO_2 is compressed to a high pressure, heated by the low-temperature recuperator (state 2), the high-temperature recuperator (state 3), and the heater (state 4), and expanded through a turbine (state 5) to produce work. In the case of the 450 MW$_e$ turbine, the expansion first occurs across a high-pressure turbine (state 5), followed by reheating (state 6 in Figure 1b), and expansion across the low-pressure turbine (state 7 in Figure 1b). The turbine exhaust is then cooled by the high-temperature recuperator (state 8), the low-temperature recuperator (state 9) and then cooled in the condenser.

Recompression occurs between the hot-side exit of the low-temperature recuperator and the cold-side inlet of the high-temperature recuperator. Only a fraction of the CO_2 is recompressed and the remaining

goes through the condenser and the main compressor. The separation between the low-temperature recuperator and the high-temperature recuperator is defined by an intermediate temperature, which is set by the exit temperature of the recompressor. The advantage of a recompression cycle is the ability to optimize recuperation. Recompression allows the two streams in the low-temperature recuperator to have different mass flows, which is used to compensate for the difference in the specific heats of the two flows.

The cycle models shown in Figure 1a and Figure 1b are simplified representations of the actual models, which include other secondary flows. Specifically, the secondary flows include various purge flows (for the main compressor, recompressor, and turbine) and seal leakage flows (turbine end seals, compressors end seals, turbine and compressor balance piston seals) that affect the cycle efficiency. The turbine balance piston is used to decrease the net thrust load for the 50 MW_e turbine, and the leakage across it bypasses the turbine. The 450 MW_e turbine is a dual-flow turbine and does not need a balance piston for thrust management. Balance piston seal leakage is thus modeled for the 50 MW_e turbine and absent for the 450 MW_e turbine. Balance piston seal leakage is modeled for the compressor/recompressor for both the 50 MW_e as well as the 450 MW_e cases. The seal leakages from the ends of the turbines and compressors leak out of the casing and expand to near atmospheric pressure. Unlike closed-loop steam Rankine cycles, low-pressure CO_2 (that has leaked past the turbine or the compressor end seal) cannot be condensed to liquid and recovered through a liquid feed pump because it's pressure is below the triple point (5.2 bar) of CO_2. Consequently, the CO_2 that has leaked past the end seal must be compressed as a vapor from near atmospheric pressure conditions back to the main compressor inlet pressure. The compression of the leaked fluid results in a penalty on the cycle efficiency, which is modeled in this work. A sub-cooler and liquid column were added to the cycle to improve the efficiency and prevent cavitation in the main compressor. The column of liquid was added by modeling the condenser to be physically located ten meters above the main compressor inlet sump.

The thermodynamic cycle design includes many component-level assumptions; these include component efficiencies, approach temperatures, leakage flows, and pressure drops. The values for these assumptions were chosen based on experience from the Sunshot design [6]. The cycle design is an iterative process, which starts with guessed values for efficiencies for turbines and compressors. The resulting cycle analysis with guessed efficiencies provides pressure, temperature and flow specifications for the turbines and compressors. The turbine design (described later in this paper) and the compressor/recompressor design (described in the companion Part-2 paper [2]) yield the actual efficiencies that are then used to update the thermodynamic cycle. Table 1 lists several key performance metrics and nominal cycle conditions for both thermodynamic cycles. The 50 MW_e cycle results in a 49.6% efficient cycle, while the 450 MW_e reheat cycle has an efficiency of 51.9%. For the 450 MW_e cycle, it was found that that reheating was responsible for an additional 1.1% efficiency gain compared to a 450 MW_e cycle without reheating. Also note that the efficiency numbers reported here assume dry gas seals for the turbine and compressor shaft-end seals (with leakage less than < 0.02% turbine mass flow) on the shaft ends of turbines and compressors. For the 450 MW_e turbine, existing sealing technology (labyrinth seals) cannot provide such low-leakage performance and remains a key technology gap for enabling the 51.9% cycle efficiency.

Table 1 Cycle parameters for the 50 MW_e and the 450 MW_e cycles

Description	50 MW_e cycle	450 MW_e cycle
Heater duty (& Reheater duty)	100.8 MW-thermal	866.3 MW-thermal
Main & Recompressor power usage	20.0 MW	162.9 MW
Cycle net electric power	50.0 MW	450.0 MW

Thermodynamic Cycle efficiency		49.6%	51.9%
State 1	Pressure	66.4 bara	65.9 bara
	Temperature	21.6^{o}C	21.5^{o}C
State 4	Temperature	488°C	545°C
State 5	Pressure	250.6 bara	250.6 bara
	Temperature	700.0^{o}C	700.0^{o}C
State 6	Temperature	-	612°C
State 7	Pressure	-	129.6 bara
	Temperature	-	680.0^{o}C
State 10	Pressure	67.2 bara	67.1 bara
	Temperature	54.9^{o}C	54.8^{o}C

3. TURBINE LAYOUT AND AERODYNAMIC FLOW-PATH DESIGN

In this section, aerodynamic flow-paths and turbine layouts are presented for the 50 MW$_e$ and 450 MW$_e$ designs. The design tool used for the aerodynamic flow-path design is a GE in-house one-dimensional (1D) aero tool, which is briefly described in this section. After this, the layout constraints for the 50 MW$_e$ design are discussed along with the turbine layout resulting from the 1D GE aero tool. Following this, the layout constraints for the 450 MW$_e$ design are discussed and the turbine layout resulting from the 1D GE aero tool is presented.

3.1 Flow-path design tool

Turbine flow-path layout is the product of an iterative process using a GE in-house 1D aero tool. The inputs to this design tool include a set of corner points defining the geometry, reaction rate and enthalpy drop for each of the stages. This is in addition to turbine speed, desired mass flow and inlet total conditions, ideal gas properties and other geometry parameters such as tip clearance and blade trailing edge thicknesses. The process is started with an approximation to flow-path geometry (corner points) along with enthalpy and reaction rates using stage loading and work coefficients as guidelines. The design calculation results in stage-by-stage flow conditions that are then compared with the target exit total pressure and exit flow angles. Subsequent iterations are made by updating the flow-path geometry, reaction rates and enthalpy drop, using the flow and work coefficients as guidelines.

The output of the 1D design tool provides the number of stages and turbine layout geometry including the number of blades, the stage axial spacing, blade radial height and the mean flow-path. Additionally, the output of the 1D tool is used to generate airfoil cross sections. Three radial cross sections were created for each blade and stacked along the center-of-gravity to create the final 3D airfoil surfaces. The 3D geometry was created only for the first and last stage blade rows to perform mechanical analysis. In the next two subsections, we describe the layout and material constraints for the 50 MW$_e$ and the 450 MW$_e$ designs.

3.2 Turbine layout for the 50 MW$_e$ scale

For the 50 MW$_e$ design, the turbomachinery technology is scaled up from the 10 MW$_e$ SwRI/GE Sunshot turboexpander [6, 7] without a complete redesign effort. One of the goals of the present work is to show scalability of the 10-MW$_e$-Sunshot architecture [6, 7] to intermediate power ratings up to 50 MW$_e$.

Due to the unavailability of high-speed generators in the 50 MW$_e$ power range, a gearbox was selected to connect one end of the high-speed rotating axial turbine to a synchronous generator. Feasibility discussions with gearbox manufacturers resulted in the conclusion that design of a 50 MW gearbox with speed reduction from 12,000 rpm to 3600 rpm is possible. On the opposite side of the turbine, a flexible coupling can be used to connect the high-speed main compressor and recompressor spinning at the same speed as the turbine. Availability of high-speed flexible couplings [10] for the power and speed range of interest was verified for both the generator as well as the compressor ends.

A key feature of the 50 MW$_e$ design is that the turbine rotor is manufactured out of a single forging of high-strength nickel alloy. This imposes a limit on the maximum turbine tip diameter due to forging size limitations. The high inlet temperature (700°C) presents challenging requirements of strength and environmental resistance, and the number of candidate alloys at these temperatures is extremely limited. Material Haynes282 (H282) was chosen within available options of other nickel-based alloys due to size availability. Long H282 forgings with diameters in the 8 to 16 inches range can be produced successfully by straight forging, whereas for forgings above 16 inches diameter, at least one upset operation needs to be considered. In order to obtain uniform grain sizes and material properties suitable for a high-speed rotating shaft, the maximum blade diameter was limited to 16 inches.

From a turbomachinery efficiency standpoint, high rotational speeds are desirable. However, oil-lubricated bearings are limited by surface speeds (typically 100 to 110 m/s), which implies that the shaft diameter (at the bearing) needs to be small to accommodate the large rotational speeds. Additionally, the torque capability (and thereby power capability) of the turbine is driven by the shaft diameter, the material strength and the fault-torque safety factor. Overall, this implies that increasing rotational speeds lead to a reduction in the bearing diameter and the torque (power) capability. For a 50 MW power transmission with H282 as the choice of rotor material, this implies that a maximum turbine speed of 9500 RPM with the corresponding shaft diameter (at the bearing) of 8.7 inches is possible.
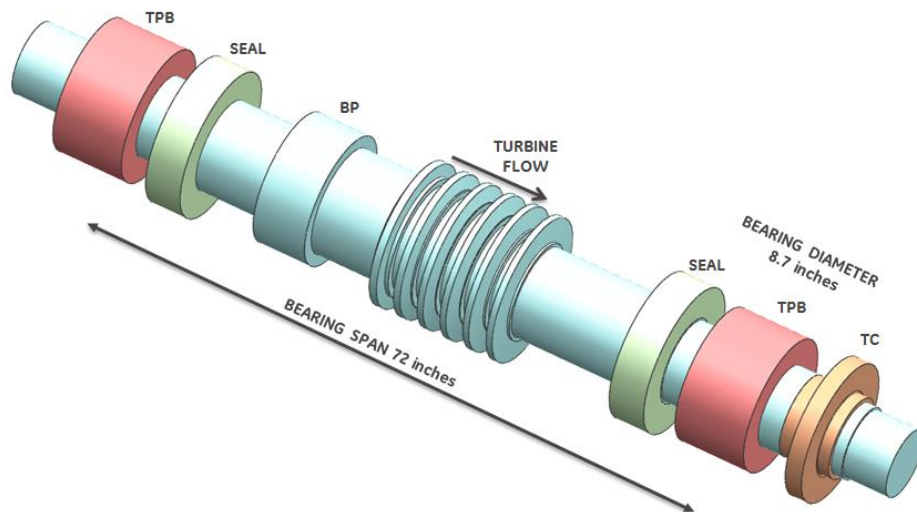

Figure 2 Solid model representation of the 50 MW$_e$ turbine rotor. TPB - tilt pad bearing, SEAL - turbine end seal, BP - balance piston, TC - thrust collar

The choice of using a single forging for the rotor combined with the forging size limitations (for H282) set an upper limit of 16 inches on the flow-path diameter. On the other hand, the bearing surface speed and material strength considerations result in a lower limit (8.7-inch bearing diameter) on the flow-path diameter along with a speed limit of 9500 rpm. These speed and flow-path constraints were combined with the flow conditions from the thermodynamic cycle to obtain an axial turbine flow-path with single-flow architecture, 6 stages, 9500 rpm and a constant 16-inch tip diameter. The resulting isentropic aero efficiency of the turbine was predicted to be 90.3%. The 50MW$_e$ turbine layout is shown in Figure 2. The mechanical analysis and axial sizing of this layout are discussed in the next section after the 450 MW$_e$ turbine layout.

3.3 Turbine layout for the 450 MW$_e$ scale

For the 450 MW$_e$ design, a clean-sheet conceptual design was performed. Several different turbomachinery layout choices were considered during the study. The primary constraint at the 450 MW$_e$ scale is that gearboxes that allow power transmission from high speeds to the two possible generator speeds of either 3600 rpm (synchronous) or 1800 rpm (sub-synchronous) are not available. Consequently, the turbine speeds are restricted to either 3600 rpm or 1800 rpm. With these two options for the turbine speed, three concepts of the turbomachinery layout exist depending on the rotational speed of the compressor and recompressor. In Table 2, three choices of shaft configuration and speed combinations are listed. It is clear that a single-shaft, single-speed layout (concept # 1) is a good compromise to achieve both efficiency and lower costs.

Table 2 Turbine-compressor architecture choices for the 450 MW$_e$ scale

Concept #	Shaft configuration	Speed	Rationale for down-selection
1	Single shaft; turbine compressors & generator on one single shaft connected to one another using couplings	3600 rpm	Both turbine & compressors run at this speed. Compressor efficiency is better than concept # 2, but less than concept # 3.
2	Single shaft; turbine compressors & generator on one single shaft connected to one another using couplings	1800 rpm	Both turbine & compressor run at this speed. The compressor efficiency is poor compared to Concept # 1 due to low speed
3	Dual shaft; turbine coupled with a generator, a separate high speed turbine coupled to the compressor	3600 rpm for one shaft, higher speed for the compressor shaft	Efficiency for the compressor is better. This option has drawbacks of additional cost associated with bearings, seals, separate turbine casings. Also starting the plant needs special equipment (additional cost)

For the 450 MW$_e$ design, a dual-flow layout was selected for both the high-pressure turbine (HPT) and the low-pressure turbine (LPT) because of the efficiency loss expected from the balance piston leakage

in a single-flow layout. Furthermore, the HPT and the LPT can be either accommodated in a single casing or split into two separate casings. The former choice leads to material cost savings and fewer components (seals, bearings) and is the preferred choice. The trade-off is that both turbines are supported on a single bearing span, which could affect the rotordynamic stability. In this paper, rotordynamic analysis (discussed later) is used to show that a configuration where both the HPT and the LPT are combined into a single casing and supported on a single bearing span is possible.

In summary, the 450 MW$_e$ layout consists of a single-shaft machine (spinning at 3600 rpm) with the LPT and HPT (both dual-flow configurations) in a single casing. These turbines are directly coupled with a compressor/recompressor train, which will be housed in a separate single casing. The 450 MW$_e$ turbine layout is shown below after discussing other layout constraints that drive the flow-path design.

Similar to the 50 MW$_e$ design, material H282 was selected for the 450 MW$_e$ turbine due to the high inlet temperature (700°C) and environmental resistance concerns associated with carbon steel (typically used in traditional steam turbine rotors). H282 forgings are available up to 44-inch diameter with 12-inch axial thickness. The small axial length of the forgings implies that neighboring stages of the turbine will need to be coupled with one another. In this aspect, the 450 MW$_e$ design is different from the 50 MW$_e$ design, where the entire turbine rotor and turbine blades (that are integral with the rotor) can be machined from a single H282 forging. Friction/bolted-flange coupling and Hirth coupling were explored as possible methods for the stage-to-stage coupling. However, these coupling choices did not show promising results. Consequently, a configuration where neighboring turbine stages are welded to form a long rotor was selected. Another key difference of the 450 MW$_e$ design from the 50 MW$_e$ design is that the 450-MW$_e$-turbine blades will be attached to the rotor using dovetails.

From a shear stress and torque capability perspective, it is desirable to choose a large turbine shaft diameter. Similar to the 50 MW$_e$ case, practical limits on bearing surface speeds and material forging sizes restrict the largest bearing diameter that can be chosen. With 110 m/s as the largest possible surface speed at the bearings, and with 3600 rpm as the rotational speed, the turbine shaft diameter at the bearing is calculated to be 23 inches. Thus, the turbine shaft diameter needs to be at least 23 inches (from the bearing diameter constraint) and turbine blade diameter can be at most 44 inches (from the material availability constraint). With additional space constraints imposed by interstage seals, the design team recommended a turbine aero flow-path with minimum blade diameter of 30 inches. These speed and flow-path constraints were combined with the flow conditions from the thermodynamic cycle to obtain a 4-stage dual-flow HPT and a 3-stage dual-flow LPT as shown in Figure 3. The bearing span is about 262 inches with a nominal shaft diameter of 26 inches resulting in a length/diameter (L/D) ratio slightly over 10. The resulting isentropic efficiency of the HPT was predicted to be 90.6% and that of the LPT was predicted to be 91.6%. In this layout (see Figure 3), the high-pressure, high-temperature CO_2 enters the turbine at the center span between the two HPTs and expands symmetrically on both sides. After expanding through the 4-stage HPT, the CO_2 is sent to the reheater and introduced again at the inlet of the LPT, where it further expands through the 3-stage LPT. The dual-flow architecture ensures that net thrust is balanced. Note that all four turbines are housed in a single casing supported on single bearing span. This architecture is possible due to the high density of CO_2. With other working fluids like steam, this type of single-casing architecture is expected to yield a larger length-to-diameter (L/D) ratio, thereby causing rotordynamic stability issues. The 3D geometries created for the first-stage HPT blade and the last-stage LPT blade are shown in Figure 4. In this next section, we discuss mechanical design aspects of the 50 MW$_e$ and the 450 MW$_e$ turbine layouts shown above.
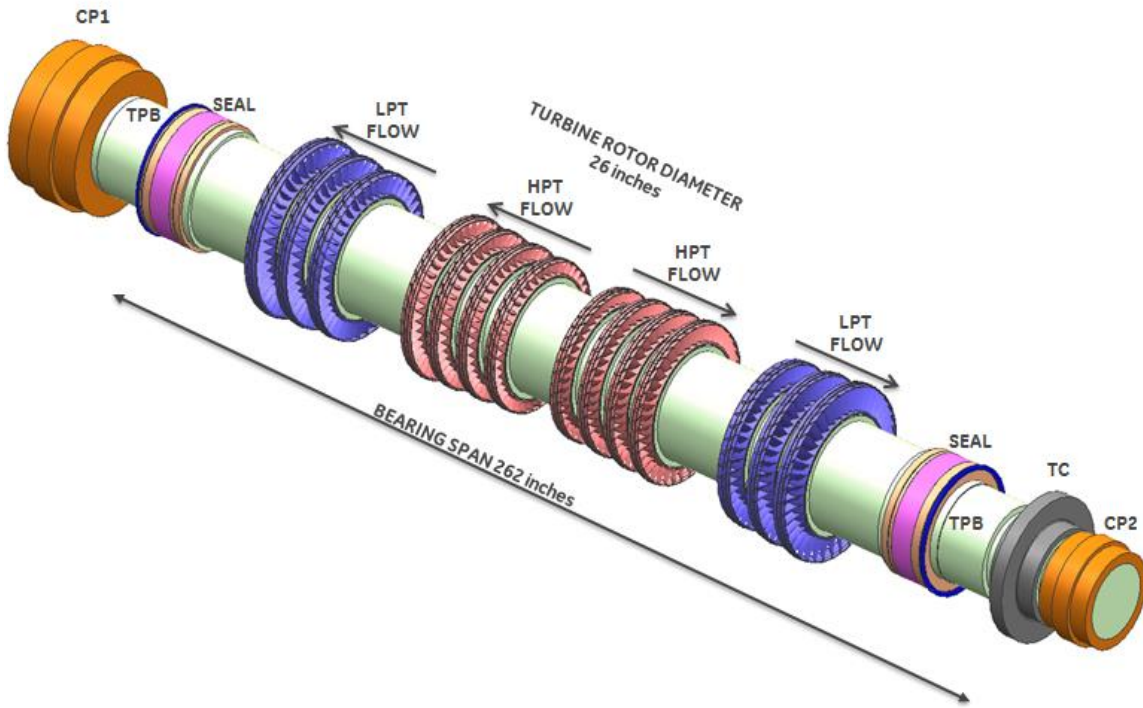
Figure 3 Solid model representation of a 450 MWe turbine concept with dual flow turbines and reheat. CP1 - generator-side coupling, TPB - tilt-pad bearing, LPT - low-pressure turbine, HPT - high-pressure turbine, TC - thrust collar, CP2 - compressor-side coupling
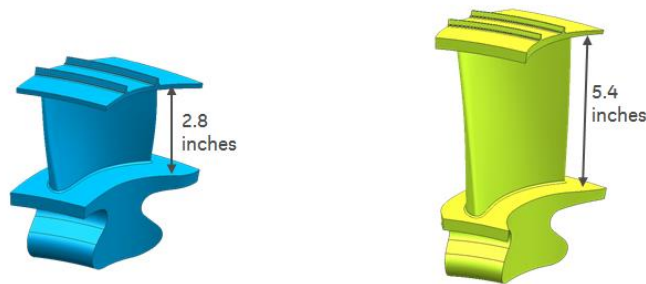

Figure 4 Solid model representation of turbine blades for the 450 MW$_e$ scale (a) 1-st stage blade of the HPT and (b) 3rd stage blade of the LPT

4. TURBINE MECHANICAL DESIGN

Following the generation of the aero flow-path discussed above, a mechanical assessment of the aero design was conducted. The assessment methodology is similar for both the 50 MW$_e$ and the 450 MW$_e$ designs.

9

Mechanical stresses induced in rotating blades by aerodynamic forces (root bending stresses) and rotational forces (pull loads) were calculated using GE Design Practices (DPs). These stresses were compared with the material limits (creep, rupture, ultimate tensile and yield properties) using criteria specified in the GE DPs. The airfoil design went through a number of iterations to meet geometric design criteria in terms of shape and form factor of the buckets. GE proprietary calculators were used for prediction of life for these blades. The final design meets the allowable stress for a specified rotor/blade life of 250,000 hours (about 30 years). Since the material H282 can withstand the stress requirements of the rotating blades, a turbine architecture where both the blades and the rotor are fabricated from a single forging of H282 was finalized for the 50 MW$_e$ design. For the 450 MW$_e$ design, the dovetail joint between the turbine blades and rotor was analyzed using GE DPs. The radial height of the dovetails was small enough to allow for a 26-inch shaft diameter with a 30-inch turbine blade inner diameter. The 3D blade geometry shown in Figure 4 for the 450 MW$_e$ design meets the life requirements design criteria defined in GE DPs.

Next, the axial sizing and rotor stress analysis is described for the 450 MW$_e$ scale. Similar sizing methodology and analysis were also used for the 50 MW$_e$ design. Apart from the axial space needed for the two LPTs and the two HPTs, the turbine rotor needs axial space for accommodating a thermal management system, the inlet and exit plenums for each turbine, the dry gas seals and the bearings. In Figure 5, the solid model of the 450 MW$_e$ turbine rotor is shown with the two LPT sections, two HPT sections, the two dry gas seals, two bearings, a thrust collar and one coupling on either side. The different axial sections of the rotor are labeled 1 through 10. A justification for the axial lengths of each of those sections is presented below.

The axial sizing of section 1 (generator coupling) and section 10 (compressor coupling) is based on F-type Ameridrives flanged sleeve coupling [10] that meet the respective torque requirements. The axial length for the section 2 (i.e. the radial tilt-pad bearing) is estimated from the bearing diameter along with typical aspect ratio for such bearings. Section 3 (i.e. the dry gas seal) is assumed to need 16 inches axial space. This assumption becomes a requirement for the seal design for this utility-scale turbine rotor.
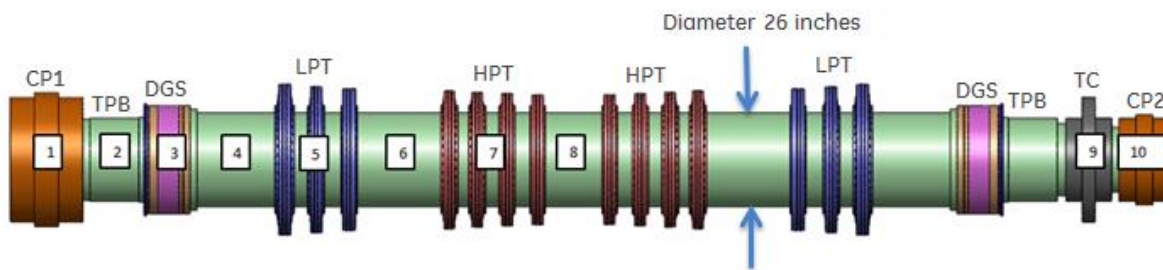

Figure 5 Solid model of the 450 MW$_e$ rotor. CP1 -- Generator Coupling, TPB -Tilt Pad Bearing, DGS - Dry Gas Seal, LPT - Low Pressure Turbine, HPT - High Pressure Turbine, TC – Thrust Collar, CP2 - Compressor Coupling

Section 4 (i.e. the LPT exit) needs to accommodate an exit diffusor (sized using GE DPs) and a thermal management section. The thermal management section is intended to reduce the axial temperature along the rotor from the LPT exit temperature to a lower temperature allowable for the dry-gas seals.

The axial space needed for Section 5 (i.e. the LP turbine) is based on the LPT flow-path design. Section 6 (i.e. the LPT inlet and the HPT exhaust) were sized using GE DPs to accommodate the HPT exit diffuser. The axial space needed for Section 7 (i.e. the HP turbine) is based on the HPT flow-path design presented earlier. Section 8 is axially sized to accommodate HPT inlet using GE DPs. Note that section 4, section 6 and section 8 also need to accommodate inlet plenums (that receive CO_2 from the heater or the reheater) and the exit plenums (that send CO_2 to the reheater or the high-temperature recuperator). Piping to the turbine casing that connects with these inlet and exit plenums were sized to minimize flow losses during operation. Since this is a dual flow machine, the thrust load is inherently balanced. For designing the thrust bearing, the thrust-bearing requirement was set such that it can support 10% of the combined one-side thrust of the HPT and the LPT. The thrust bearing was sized by scaling commercially available thrust bearings [11]. Overall, this leads to a turbine rotor of axial length (bearing to bearing) of about 262 inches with L/D ratio slightly above 10. Next, the stress calculations for the rotor are described followed by the rotordynamic stability analysis.

Using the power produced at every turbine stage, the power supplied to the generator and the power consumed by the compressors, a torque diagram of the turbine shaft was generated. This torque diagram is shown in Figure 6 along with the layout of the turbine rotor. The shear stress induced by the torque is calculated at different axial locations and is also plotted in Figure 6. Apart from this shear stress, the rotor is also subjected to axial stress caused by the thrust load, radial stress caused by a combination of blade pull loads and centrifugal loads, and a tangential hoop stress due to rotation. Stress calculations combining these different loads show that the rotor has margin against creep failure and an adequate factor of safety for the torque-induced shear stress. Overall, from a stress perspective, a 3-stage dual-flow LPT and a 4-stage dual flow HPT turbine is feasible. A rotordynamic stability analysis of the 450 MW$_e$ turbine rotor is presented next.
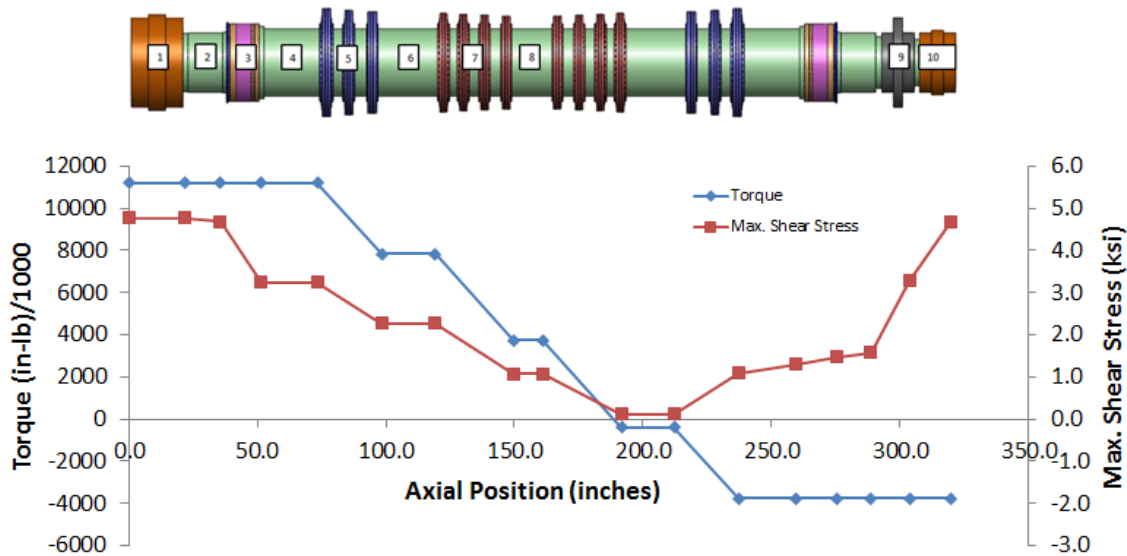

Figure 6 Torque and shear stress distribution at various axial locations of the rotor

Rotordynamic stability of the 450 MW$_e$ turbine rotor was analyzed using the XLTRC2 software developed by Texas A&M University [12]. The solid model of the 450 MW$_e$ turbine rotor was used as a starting

point for geometry definition. The turbine rotordynamic model is shown in Figure 7. Beam elements were used to model the rotor stiffness, and lumped inertia values were used to model the turbine blades. Mass-only elements were used for the thrust disk and coupling half-weights were added as mass. Tip seals and interstage seals were modeled using GE and SwRI design practices. Tilt-pad journal bearings were used with bearing stiffness calculations performed using THPAD bearing code, which is part of the ROMAC rotordynamic codes. Three different rotordynamic configurations were analyzed: (a) a configuration with rigid bearing support, (b) a configuration with rigid bearings and reduced coupling weight, and (c) a configuration with soft support and squeeze film dampers. The results of these analyses are briefly described below.

The undamped critical speed map for the turbine rotor with a rigid bearing support shows that the first mode (1000 rpm) and the third mode (4600 rpm) are away from the operating speed (3600 rpm), but the second mode (3400 rpm) is very close to the operating speed. We analyzed the forced response of this system and found that without any seals (interstage or tip seals), the second mode response does not meet the required separation margin requirements per API standards [13] (required separation margin is 12.8% versus actual separation margin of 5.6%). Addition of seals (tip seals and interstage seals) along with their force coefficients did not improve the separation margins. Finally, inclusion of swirl brakes to these seals did not improve the separation margins either. A stability analysis for the case with swirl brakes showed good stability margin. Overall, this rotordynamic configuration with rigid bearing support (with seals and swirl brakes) showed good stability margin, but did not have the API-required separation margins for the second mode forced response.
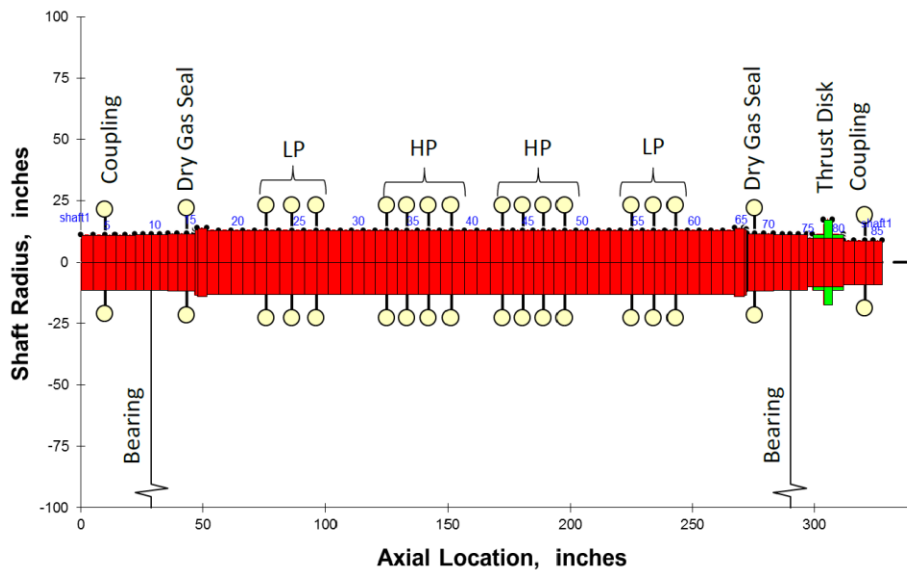

Figure 7 Rotordynamic model for the 450 MW$_e$ turbine

In the second configuration, sensitivity studies were performed to study the effect of the coupling weight. In the original configuration discussed above, the generator-side coupling (which transmits 450 MW power) weighed about 6600 lb (half-weight). An alternate coupling with the same torque/power rating but with a 1600 lb half weight was designed and modeled in the rotordynamic study. The reduced weight of the generator-side coupling had a significant impact on the turbine rotordynamics. Specifically, a modified turbine configuration that included a reduced-weight coupling was analyzed

without modeling the effects of seals (tip seals or interstage seals). For the first three modes, the forced response of the rotor showed adequate separation margin as required by the API standard [13]. Consequently, a rotordynamic configuration with rigid bearings but a reduced-weight coupling (approximately ¼ half-weight) can make the turbine rotordynamics acceptable.

As an alternate to the second configuration described above, a third rotor configuration was analyzed with soft bearing supports and squeeze film damper. It is difficult to estimate the exact foundation stiffness for the bearings because a turbine casing has not yet been designed for the 450 MW$_e$ turbine concept. Using experience-based correlations, the combined bearing stiffness (bearing fluid film stiffness in series with the foundation stiffness) was estimated to be $1e^6$ lb/inch, which is about 3 to 4 times lower than just the bearing film stiffness. In combination (parallel) with this reduced bearing stiffness, squeeze film dampers were added with a nominal damping of 15000 lb-s/inch. The undamped critical speed map for this configuration shows that the first three modes of the turbine rotor are at 800 rpm, 1200 rpm and 2400 rpm compared to the operating speed of 3600 rpm. The fourth mode is higher and sufficiently separated from the operating speed. The forced response of the rotor shows adequate separation margin for the first three modes (to meet the API requirements [13]) and seals with swirl brakes provide good stability margin. Overall, this configuration with soft-mounted bearings and squeeze film dampers is another alternative configuration to ensure that the turbine rotor has acceptable rotordynamic behavior.

Overall, this section described stress analysis for the turbine blades, blade-attachment method, stress analysis for the turbine rotor and a rotordynamic analysis for the turbine rotor. Based on these preliminary analyses, the turbine rotor has an acceptable mechanical design.

5. TECHNOLOGY GAPS FOR UTILITY-SCALE sCO2 TURBINES

The 450 MW$_e$ turbine rotor concept described in this paper is a single-shaft, single-casing layout that operates at 3600 rpm and is based on a reheat, recompression cycle. The thermodynamic efficiency of this cycle is 51.9%. While this efficiency is higher than state-of-the-art ultrasupercritical steam turbines, there are challenges in realizing this performance. These challenges include high-temperature furnace design, optimization of heat exchangers, turbine end sealing technology and thermal management with supercritical CO_2. These challenges are briefly described below.

As shown in Table 1, this work assumes that it is possible to add heat to the power cycle in a furnace with CO_2 feed temperatures of about 500°C or greater and exit temperatures of about 700°C with 250 bar pressure. Conceptual designs of primary heater that demonstrate this capability are needed to confirm this assumption. Furthermore, high-temperature flue gas heat recovery systems, such as regenerative air preheaters (that operate with 550°C flue gas) are beyond the state-of-the-art technology for coal power plants. It is desirable to address these furnace design challenges to ensure that utility-scale sCO$_2$ power generation is competitive with steam turbine technology.

The analysis in this paper found that the efficiency gain with reheat is sensitive to the component pressure drops assumed in the cycle. Specifically, the cycle efficiency is sensitive to: (a) the pressure losses in the HPT diffuser, (b) the pressure losses in the reheater, and (c) the pressure losses in the LPT inlet plenum. For example, an additional 1% DP/P pressure loss in the reheater reduces the cycle efficiency by about 0.3 points. Concept designs for reheater systems with low pressure drops are desirable to maximize the cycle efficiency of utility-scale sCO$_2$ power cycles that utilize reheat.

Finally, the high cycle efficiency reported in this paper is enabled by dry gas shaft end seals that leak less than 0.02% of the turbine mass flow through the end seals of the turbine. The existing sealing

technology for large-diameters (24-inch) and high-differential pressures (> 75 bar) is labyrinth seals. With labyrinth seals, the leakage past two end seals (one on either end of the turbine) was estimated to about 0.45% of the overall turbine mass flow. Thus, the leakage loss with existing sealing technology is more than an order of magnitude higher than the desirable low leakage, which can be achieved using dry gas seals. This large leakage using existing labyrinth seals can reduce the cycle efficiency by 0.6 to 0.8% points, which negates much of the potential advantage relative to the incumbent steam cycle. Thus, it is desirable to develop large-diameter, high-pressure and low-leakage dry gas seals for ensuring high efficiencies and competitiveness of utility-scale sCO_2 power cycles over steam turbine technology.

6. SUMMARY AND CONCLUSIONS

In this paper, two thermodynamic cycles were presented along with turbine layouts for the 50 MW$_e$ and the 450 MW$_e$ scales. The 50 MW$_e$ thermodynamic cycle leveraged previous SwRI/GE Sunshot CSP cycle with important modifications including CO_2 condensation to improve efficiency. The 50 MW$_e$ cycle resulted in a cycle efficiency of 49.6%. For the 450 MW$_e$ scale, the thermodynamic cycle was further modified to include reheating, which improved the cycle efficiency by 1.1% over the non-reheat case. The 50 MW$_e$ turbine is a scaled-up version of the 10 MW$_e$ SwRI/GE Sunshot turbine and demonstrates that the 10 MW$_e$ architecture is scalable to intermediate power ratings. The 450 MW$_e$ turbine is an assembled rotor with a dual-flow layout with both the HPT and the LPT housed in single casing and supported on a single bearing span. In this work, the turbine layouts were designed using aerodynamic flow-path considerations and demonstrated to be mechanically feasible for the choice of H282 material. Overall, the conceptual designs hold promise subject to the technology gaps discussed in this paper. Further optimization of these concepts from an economic standpoint could result in modified architectures.

ACKNOWLEDGEMENT

DISCLAIMER

REFERENCES

[1] Y. L. Moullec, "Conceptual study of a high efficiency coal-fired power plant with CO2 capture using a supercritical CO2 Brayton cycle," vol. 49, pp. 32-46, 2013.

[2] R. A. Bidkar, G. Musgrove, M. Day, C. D. Kulhanek, T. Allison, A. M. Peter, D. Hofer and J. Moore, "Conceptual Designs of 50MWe-450MWe Supercritical CO2 Turbomachinery Trains for Power Generation from Coal. Part 2: Compressors," in *The 5th International Symposium - Supercritical CO2 Power Cycles*, San Antonio, TX, 2016.

[3] S. A. Wright, T. M. Conboy, E. J. Parma, T. G. Lewis, G. A. Rochau and A. J. Suo-Anttila.

[4] E. M. Clementoni, T. L. Cox and C. P. Sprague, "Startup and Operation of a Supercritical Carbon Dioxide Brayton Cycle," *J. Eng. for Gas Turbines and Power,* vol. 136, p. 071701, 2014.

[5] A. Kacludis, S. Lyons, D. Nadav and E. Zdankiewicz, "Waste Heat to Power Applications using a Supercritical CO2-based Power Cycle," in *Power Gen International* , Orlando, FL, 2012.

[6] J. J. Moore, K. Brun, N. Evans, P. Bueno, C. Kalra, D. Hofer, T. Farineau, J. Davis, L. Chordia, B. Morris, J. McDonald and K. Kimball, "Development of a High Efficiency Hot Gas Turbo-expander and Low Cost Heat Exchangers for Optimized CSP sCO2 Operation," in *KAPL sCO2 Workshop*, Niskayuna, NY, 2014.

[7] C. Kalra, D. Hofer, E. Sevincer, J. Moore and K. Brun, "Development of High Efficiency Hot Gas Turbo-expander for Optimized CSP sCO2 Power Block Operation," in *4th International sCO2 Power Cycles Symposium*, Pittsburgh, PA, 2014.

[8] J. J. Sienicki, A. Moisseytsev, R. L. Fuller, S. A. Wright and P. S. Pickard, "Scale Dependencies of Supercritical Carbon Dioxide Brayton Cycle Technologies and the Optimal Size for a Next-Step Supercritical CO2 Cycle Demonstration," in *Supercritical CO2 Power Cycle Symposium*, Boulder, CO, 2011.

[9] NETL, US DOE, "Cost and Performance Baseline for Fossil Energy Plants, Volume 1," DOE/NETL-2010/1397, Pittsburgh, PA, 2010.

[10] "Ameridrives Couplings," Altra Industrial Motion Group, 2015. [Online]. Available: www.ameridrives.com.

[11] "Waukesha Bearings," Waukesha Bearings Corporation, 2015. [Online]. Available: www.waubearing.com.

[12] The Turbomachinery Laboratory, Texas A&M University, 2014. [Online]. Available: http://turbolab.tamu.edu.

[13] API Standard 617, Axial and Centrifugal Compressors and Expander-Compressors for Petroleum, Chemical and Gas Industry Services, Washington, D.C.: American Petroleum Institute, 2002.

AUTHOR BIOGRAPHIES

Dr. Rahul Bidkar is a Mechanical Engineer at GE Global Research Center in Niskayuna, NY. He received his Ph.D. in Mechanical Engineering from Purdue University. At GE, Rahul has led development of several film-riding turbomachinery seals with applications to aircraft engines, gas turbines, steam turbines and supercritical CO_2 turbines along with coatings development work for fluid drag reduction. He has authored over 10 technical papers, 14 patent applications with 4 granted patents.

Andrew Mann is an Energy System Engineer at General Electric Global Research. His research in on the thermodynamic and economic modeling of power generation systems, with recent focus on supercritical CO_2 cycles. He received his master's degree from Stony Brook University in 2013.

Mr. Sevincer is currently a Mechanical Engineer in the Mechanical Systems Organization at GE Global Research Center. His research interests are in the areas of design and development of Turbomachinery components, sealing systems for aircraft engines, gas & steam turbines. At GE Global Research, Mr. Sevincer has been involved in the development of analytical tools used for combustor design characterization, mechanical design & optimization of gas turbine components, design, development and testing of Multiphase pumps and pumping systems in addition to developing new sCO_2 turbine concepts for Sunshot program.

Stefan Cich is a Research Engineer in the Mechanical Engineering Division at Southwest Research Institute in San Antonio, TX. He received his B.S. in Aerospace Engineering from the University of Texas at Austin. His main focus while at SwRI has been on the design, analysis, and manufacturing of turbomachinery casings and rotor layouts. Recent work has been in the design of a 10MW supercritical CO2 turbine under the DOE Sunshot program.

Meera Day is an Engineer in the Rotating Machinery Dynamics Section at Southwest Research Institute in San Antonio, TX. While at SwRI, her research has included instrumentation, performance testing, control systems, and rotordynamics analysis intended for applications such as turboexpanders, centrifugal compressors, and utility scale cycles. She has Bachelor of Science degrees in Mechanical Engineering and Mathematics from Southern Methodist University.

Dr. Azam Thatte is a Lead Research Engineer at GE Global Research Center in Niskayuna, NY. He received Ph.D. in Mechanical Engineering from Georgia Tech in 2010. His research interests include multi-scale multi-physics modeling, fluid-structure interaction, aircraft engine design, turbomachinery flows, hydrodynamic film riding sealing and gas bearing technology. Currently Dr. Thatte is the Principal Investigator of a large U.S. DOE research program on developing coupled-physics performance and life prediction models and material models for supercritical CO_2 turbomachines. He has developed novel experimental methods to characterize thermodynamics of phase transition in CO_2 and to study effect of chemical kinetics of CO_2 on 3D fracture mechanics in superalloys. He has authored more than 30 journal & peer reviewed conference publications including one in Nature. He has also filed 12 patent applications.

Dr. Peter is a Principal Engineer at GE Global Research Center in Niskayuna, NY. He received his Ph.D. in Aeronautical Engineering from the University of Washington. While at GE, he has worked on gas turbines, fuel cells, boiling water nuclear reactors, concentrating solar power, and supercritical CO_2 turbomachinery. He has also been a product line leader for GE's Integrated Solar Combined Cycle system.

Dr. Douglas Hofer is a Senior Principal Engineer at the GE Global Research Center in Niskayuna NY. His research interests are in the areas of turbomachinery aero-thermal fluid dynamics, advanced expander and compressor technologies, two-phase flows, non-ideal gasses, and transonic and supersonic flows. He has deep experience in the steam turbine industry both in turbomachinery design and cycle analysis and innovation.

Dr. Jeffrey Moore is an Institute Engineer in the Machinery Section at Southwest Research Institute in San Antonio, TX. He holds a B.S., M.S., and Ph.D. in Mechanical Engineering from Texas A&M University. His professional experience over the last 25 years includes engineering and management responsibilities related to centrifugal compressors and gas turbines at Solar Turbines Inc. in San Diego, CA, Dresser-Rand in Olean, NY, and Southwest Research Institute in San Antonio, TX. His interests include advanced power cycles and

compression methods, rotordynamics, seals and bearings, computational fluid dynamics, finite element analysis, machine design, controls and aerodynamics. He has authored over 30 technical papers related to turbomachinery and has two patents issued and two pending. Dr. Moore is the Vanguard Chair of the Structures and Dynamics Committee and has held the position of Oil and Gas Committee Chair for IGTI Turbo Expo. He is also the Associate Editor for the Journal of Tribology and a member of the IGTI SCO2 Committee, Turbomachinery Symposium Advisory Committee, the IFToMM International Rotordynamics Conference Committee, and the API 616 and 684 Task Forces.